Asian Journal of Nanoscience and Materials 4 (2021) 1-14

Asian Journal of Nanoscience and Materials

Journal homepage: www.ajnanomat.com

Original Research Article

Surface potential, fermi level and band gap energy of copper doped magnesium nickel ferrite nanoparticles

Gideon Osamong[a], Paul Kuria Kamweru[a,*], Joel Mwangi Gichumbi[a], Francis Gichuki Ndiritu[b]

[a] *Department of Physical Sciences, Chuka University, Chuka, Kenya*

[b] *Registrar Academic Affairs, Chuka University, Chuka, Kenya*

ARTICLE INFORMATION

Received: 30 June 2020
Received in revised: 15 September 2020
Accepted: 27 September 2020
Available online: 26 October 2020

DOI: 10.26655/AJNANOMAT.2021.1.1

KEYWORDS

Band gap energy
Fermi level
Surface potential
Nanoferrites

ABSTRACT

Optical, electrical, and electronic properties of materials are essential in the fabrication of electronic devices. These properties can be improved through doping and reduction of the size of a material to nanoscale. In this study, copper doped magnesium-nickel ($Cu_xMg_{1-x}NiFe_2O_4$, for x=0.00, 0.15, 0.30, 0.45, 0.60, 0.75, 1.00) ferrite nanoparticles were synthesized using the citra-gel auto combustion method. The electronic and optical properties were evaluated using the scanning Kelvin probe microscopy (SKPM) and UV-visible, respectively. The UV-visible studies revealed that, the band gap energy was at the range of 3.600-3.750 eV. The band gap was noted to increase with copper content up to x=0.45 which then started to decrease. The undoped sample displayed the lowest band gap energy in comparison with the doped. SKPM analysis exhibited the surface potential in the range 4.361-5.002 eV for the area scan and 4.251-5.006 eV for the line scans for the samples. The sample with x=0.75 showed a positive work function for both area and line scans, and all the others had a negative work function. The doped ferrite exhibited the properties that could be applied in optical devices, storage devices, and recording devices.

Corresponding author, email: pkamweru@gmail.com (Kamweru P.K.).
Tel.: +254726320644.

Graphical Abstract

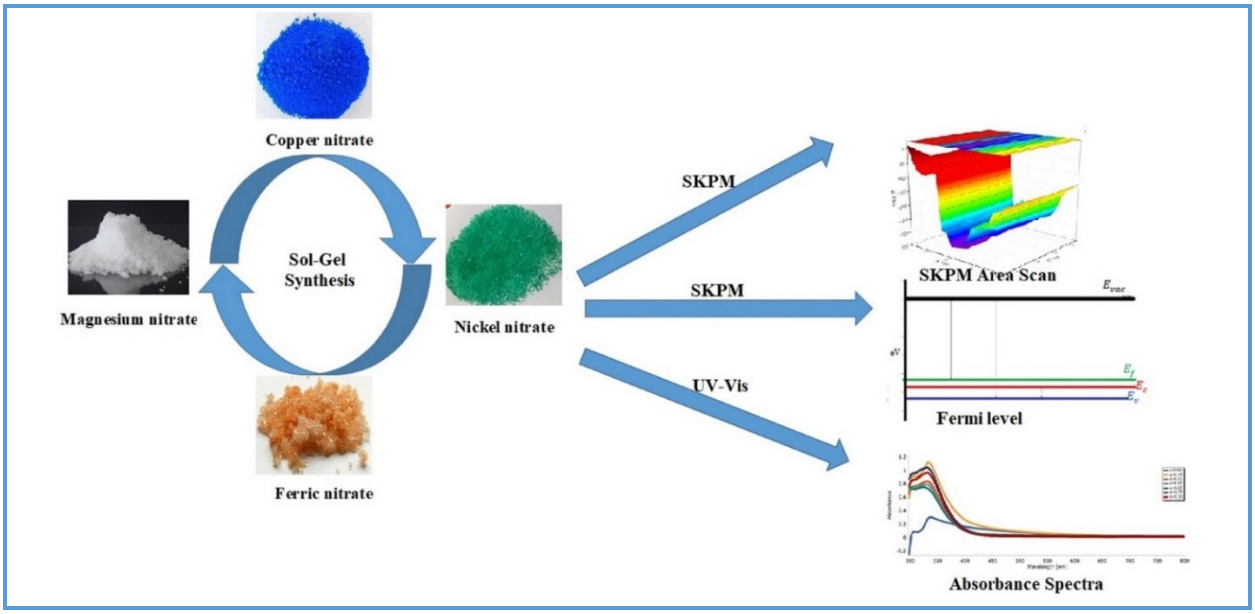

Introduction

Efforts are currently being made to develop novel materials with low power loss to be applied in the miniaturization of electronic devices [1]. One such material is ferrite nanomaterial which can aid in miniaturization. Ferrites exhibit novel optical, magnetic and electrical properties [2, 3]. This makes the nanoferrites a base material for several technological, industrial and scientific applications [4], for example, the Li-ion batteries superconductors [5, 6], flexible recording media [7, 8], EMI shielding [9], and magnetic refrigerators [10]. Among the ferrites, spinel ferrite has elicited much interest in the electronics and telecommunication industry due to its low eddy current losses, high permeability, magneto-resistive and magneto-optical properties and high electrical resistivity. Minute particles have a unique atomic structure with discrete electronic states which give rise to important properties in addition to the superparamagnetic behavior. Nano ferrites are usually doped to improve the desirable electrical properties [11, 12]. This can be achieved by using nanotechnology, a classical scientific discipline which involves fields such as material science, chemistry, electronics and mechanics, in the development of functional systems materials and equipment with novel properties emanating from the ability to self-organize matter in nanometer scale and form the quantum principles [13].

Copper ferrite which is a p-type semiconductor is an example of spinel ferrite, it has important properties such as environmental stability, electrical, optical, electrochemical, chemical and thermal stability [14]. It crystallizes in either cubic or tetragonal phases, where the cubic phase is stable at higher temperatures. Considering these properties, it can be used in many applications including, catalytic, gas sensing, high-density storage devices, and anode for Li-batteries [15]. Magnesium ferrite is another spinel ferrite, which is an n-type semiconductor material. It has a series of applications such as sensors, adsorptions, and the magnetic technologies [16]. Nickel ferrite is a spinel ferrite with high

electrical resistivity, mechanical hardness and chemical stability besides having a reasonable cost [17]. Given these properties, it will be interesting to synthesize mixed nanoferrites of copper nickel and magnesium and determine their optical and electronic properties.

Mixed ferrites have shown improved properties such as coercivity and saturation magnetization as compared to the pure ferrites [18]. Enhanced magnetic properties have been observed in Ni-Co-Zn ferrite which makes them useful ferromagnetic core materials. Chemical stability, mechanical hardness and high electrical resistivity have also been observed in polycrystalline ferrites which find applications in electronic devices. Electronic devices should possess high resistivity as possible to minimize the eddy currents that contribute to heat loss. This can be achieved in ferrites where crystalline boundaries act as barriers hence confining charge carriers [19].

Electronic configurations vis a vis energy levels of a material such as the work function, vacuum level, electron affinity, and fermi level are essential parameters in device fabrications [20]. These electronic properties are dependent on the factors such as surface constriction, chemical composition, and number of contaminants on the surface of the material in place. Therefore, material of the same type but different orientation can have different surface potential and fermi level.

Surface potential is an important factor in material science to be contemplated in material fabrication for use in memory and storage devices among other electronic applications [21]. It is a basic electronic property defined as the minimum amount of energy needed to remove an electron from the level into a vacuum level. It depends on the nature of a material crystalline surface. Surface potential values are used to determine properties of materials to be applied in diodes, Schottky barriers and computer memory devices [22]. The electron surface potential is the least amount of energy required to dislodge an electron from the surface of a solid to a point in the vacuum just outside the solid surface, at zero kinetic energy [8]. High surface potential implies high surface energy, disordered grains have got lower surface energies as compared to crystal grains [23], this is because higher attraction of a crystallographic grain with a low surface potential may result in higher mobility of electron [24].

Scanning Kelvins Probe Microscopy is a novel technique for determining work function for metals or surface potential for semiconductors, between a conducting sample and the vibrating tip [25]. It is a non-contact and non-destructive technique that gives information about surface structure and surface composition of a material. Besides, the surface defects like vacancies can be imaged by the Kelvins probe [26, 27]. This technique uses both the Kelvins method and Einstein's photoelectric effect to produce absolute surface potential in electron volts. The electron surface potential interrelates to material mechanical, optical, electrical and structural properties. Therefore, the surface potential is a high measure of the surface condition which is affected by absorbed or evaporated layers, surface regeneration, surface charging, oxide coating imperfections surface and bulk contaminations among others.

The energy band gap which is somehow related to the work function is another important parameter that determines the electrical conductivity of a material. It is the amount of energy that is needed by a valence electron to jump from the valence band to the conduction band which makes the electron free to move within the crystal surface otherwise known as the charge carrier [28]. Therefore, the band gap of ferrites is critical for surface science, nanomaterial, electronic and solar

industry applications [29]. In ferrites, charge carriers are not free to move through the crystal lattice but instead jump from ion to ion [30]. Ideally band gap refers to the difference in energy between the top of the valence band and bottom of the conduction band. The fundamental absorption energy which corresponds to electron excitation from the valence band to the conduction band, can be used to determine the band gap of the synthesized samples. The UV-visible gives the absorption peaks which is equivalent to the energy absorbed by an electron at a specific wavelength. The absorbed energy makes the electron to be excited from the ground state thus creating a band gap [31].

In this work we have synthesized copper doped magnesium nickel ferrite nanoparticle using Citra gel auto combustion method. Characterization has been done using Kelvins probe and UV-visible to determine work function and band gap energy respectively.

Experimental

The following nitrates of analytical grades were used, nickel nitrate hexahydrate (Ni $(NO_3)_2.6H_2O$), copper nitrate trihydrate (Cu $(NO_3)_2.3H_2O$), ferric nitrate nanohydrate (Fe $(NO_3)_3.9H_2O$) and magnesium nitrate hexahydrate (Mg $(NO_3)_2.6H_2O$). The ferrite sample of copper doped magnesium nickel ($Cu_xMg_{1-x}NiFe_2O_4$, for x=0.00, 0.15, 0.30, 0.45, 0.60, 0.75, 1.00) nanoparticles were prepared through Citra-gel auto combustion method. The required amount of each metal nitrate was dissolved separately in distilled water under magnetic stirring. Citric acid solution was prepared separately of mole ratio 1:1 to the metal nitrates. It was then mixed with the nitrate solution under heating and magnetic stirring at a temperature of 110 for 3 h with the addition of an ammonia solution to maintain the pH at 7. After gel was formed, heating was continued to auto combustion to form loose powders. The powder was calcined at 700 °C in a marble furnace and crushed to fine powder. The work function and fermi level analysis were done using SKPM. A few drops of polyvinyl alcohol (PVA) were added to the calcined nanoferrites powder to act as a binder. The bound powder samples were compressed into a disc shape of diameter about 1cm, with help of a manual hydraulic press. The surface potential of the compressed discs of the ferrite was probed using the Ambient® Kelvin probe manufactured by KP Technology. This was done at a gradient of 300 and approximately 2V peak to peak voltage for 20 points. The Kelvin probe was calibrated using a gold sample, thereafter the samples were loaded into the sample holder for scanning to obtain their contact potential difference between the samples and the tip. The surface simulations as well as the band energy diagram were plotted using KP Wize software from Kp technology. The optical analysis was done using UV-Visible 1800 series to obtain the absorbance at a slit width of 1 nm and a wavelength of 340 nm. The sintered powders were dissolved in pyridine and ethylene glycol in the ratio 1:10. under magnetic stirring. The sample solutions were loaded into the cuvette to obtain the absorbance spectrum.

Results and Discussions

Work function and fermi level

Both the line scan and area profile for the work function of the synthesized samples are as shown in Figure 1–7. The convex parts correspond to peaks while concave to the valley in the surface profiles. The atoms are constrained in the valley and electrons are bound by the surrounding atoms making it difficult for the electron to escape.

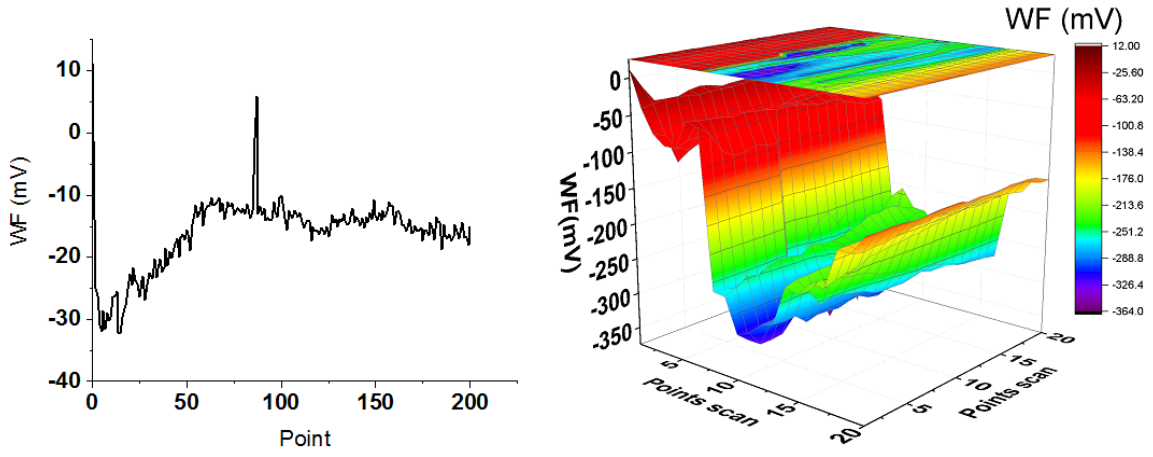

Figure 1. Surface potential for line scan and area profile of $MgNiFe_2O_4$ with work function 4.684 eV and 4.524 eV, respectively

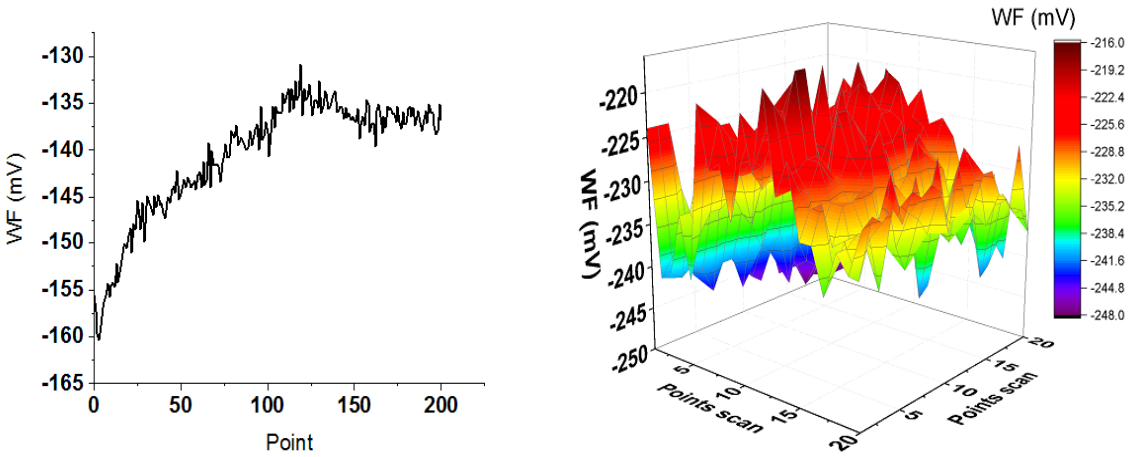

Figure 2. Surface potential for line scan and area profile of $Cu_{0.15}Mg_{0.85}NiFe_2O_4$ with work function 4.560 eV and 4.469 eV, respectively

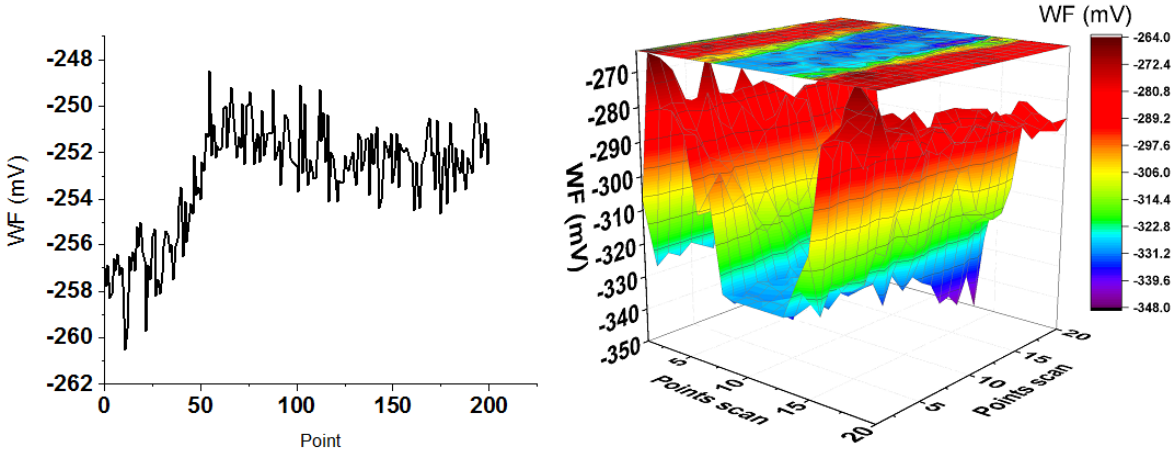

Figure 3. Surface potential for line scan and area profile of $Cu_{0.30}Mg_{0.70}NiFe_2O_4$ with work function 4.251 eV and 4.394 eV, respectively

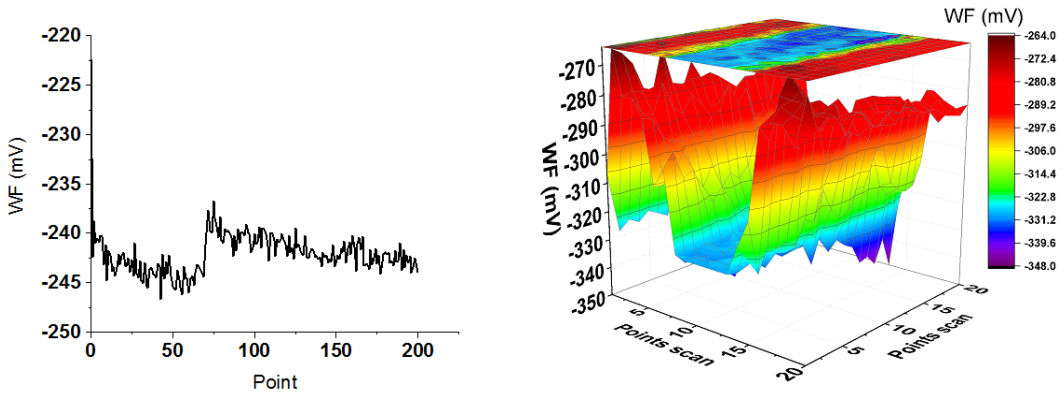

Figure 4. Surface potential for line scan and area profile of $Cu_{0.45}Mg_{0.55}NiFe_2O_4$ with work function 4.458 eV and 4.459 eV, respectively

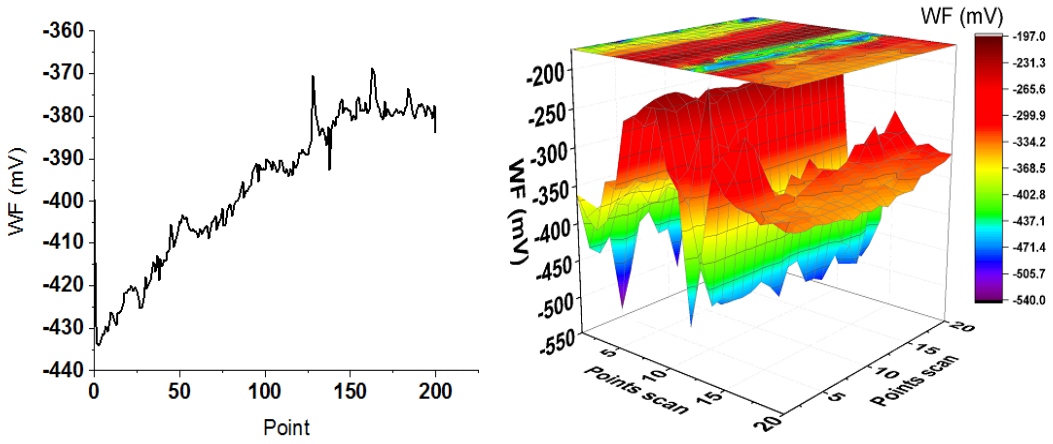

Figure 5. Surface potential for line scan and area profile of $Cu_{0.60}Mg_{0.40}NiFe_2O_4$ with work function 4.304 eV and 4.361 eV, respectively

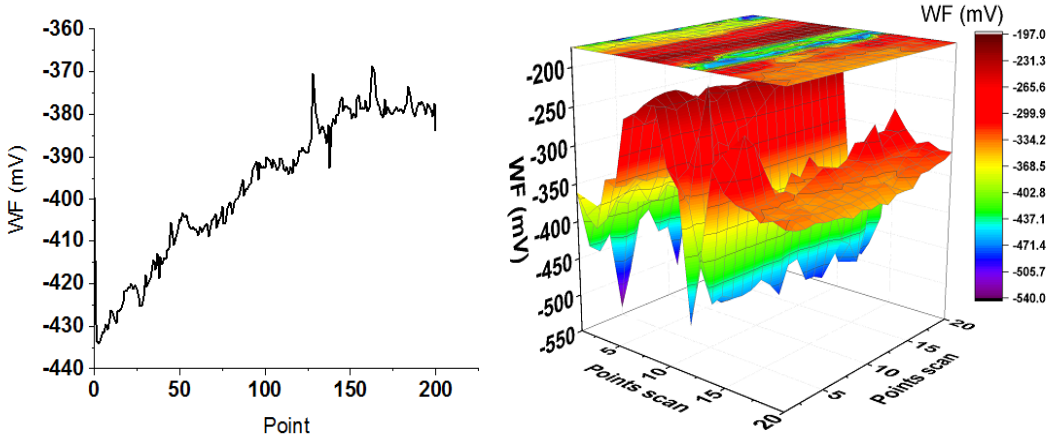

Figure 6. Surface potential for line scan and area profile of $Cu_{0.75}Mg_{0.25}NiFe_2O_4$ with work function 5.006 eV and 5.002 eV, respectively

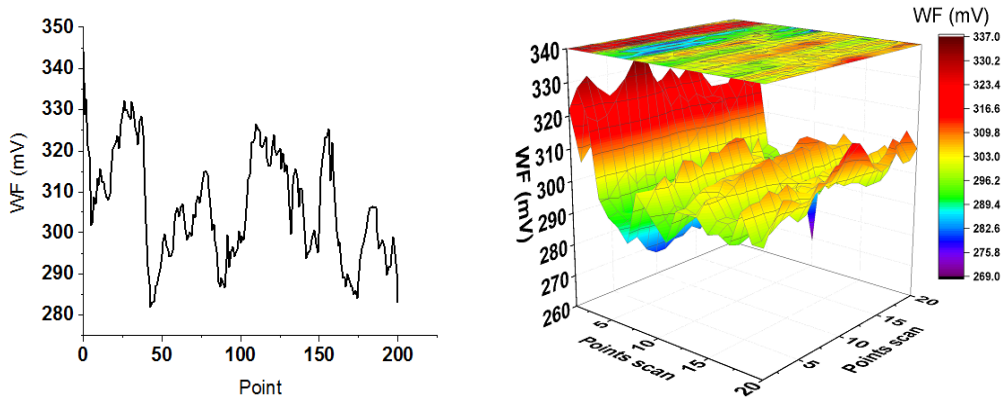

Figure 7. Surface potential for line scan and area profile of $CuNiFe_2O_4$ with work function 4.596 eV and 4.529 eV, respectively

All samples depicted a negative work function with an exception of sample $Cu_{0.75}Mg_{0.25}NiFe_2O_4$ which showed a positive work function for both the line scan and surface profiles. The negative work function revealed that the work function of the sample is lower than that of gold used in the calibration of kelvins probe while the positive work function shows that the work function of the sample is higher than that of gold. The lowest work function for area scan is 4.361 eV for the sample x=0.60 and the highest was 5.002 eV, for x=0.75. For the line scan the lowest is 4.251 eV for the sample x=0.30 and the highest was 5.006 eV for the sample x=0.75. It worth noting that the highest work function for both area and line scans was recorded in the sample x=0.75. This shows that copper doping shifts the work function, thus suggesting the Ohmic nature of the copper doped magnesium nickel ferrite nanoparticles. The surface formation or reconstruction could be an issue to account for the variation of the work function [32]. There is an observed variation in the work function, as seen in Figure 1–7. This variation may be caused by several factors such as the surface morphology, chemical composition of the sample and the structure of the material [20]. For instance, a shift in the surface molecular orientation of a sample or a small amount of contaminant on the surface can bring a significant shift in the work function and impact the electronic structure of interfaces. Electrons can easily escape the surface due to reduced bonding. Studies have indicated that the rough the surface the larger the fluctuation in the work function [14]. The samples also show the Schottky junction type of semiconductor material. This is consistent with the work done by [33]. This can be predicted from the size of the band gap or the height between the fermi level and the conduction band. The surface potential for the doped samples was calculated using Equation 1 [34].

$$Q_S = Q_{tip} + CPD \quad (1)$$

Where, CPD is the contact potential difference, Q_{tip} work function of the tip and Q_S surface potential of the sample. The plot for both line and area scans are as demonstrated in Figure 8.

Copper doping varies surface potential. These surface potential values reveal the semi-conductivity nature of the synthesized samples brought about by the doping effect. The work function is a key metric that determines the charge transfer across the interface of devices in the electronic industry. The energy band diagrams are, as shown in Figure 9–12.

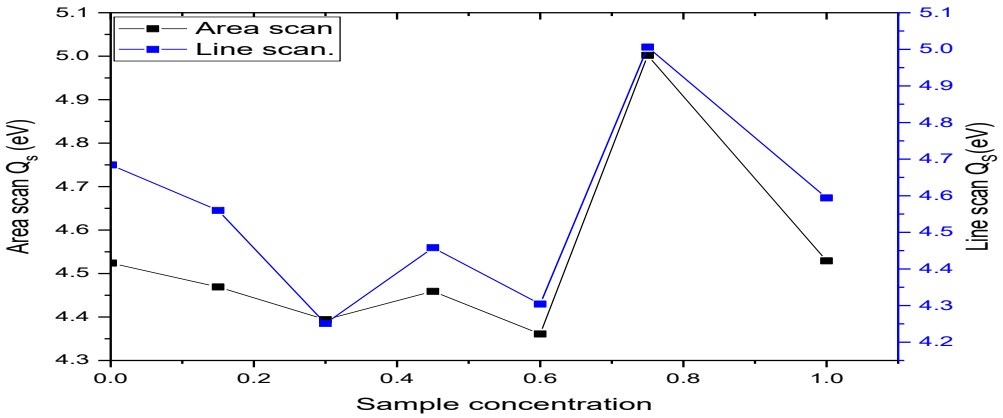

Figure 8. Surface potential for both area and line scan of $Cu_xMg_{1-X}NiFe_2O_4$ (for x=0.00, 0.15, 0.30, 0.45, 0.60, 0.75 and 1.00) for. It shows that copper doping has an effect on surface potential

Figure 9. a) Energy band diagram for sample $MgNiFe_2O_4$. The fermi level has shifted towards the conduction, a characteristic of an n-type semiconductor. b) Energy band diagram for sample $Cu_{0.15}Mg_{0.85}NiFe_2O_4$. The fermi level has shifted towards the conduction, a characteristic of an n-type semiconductor

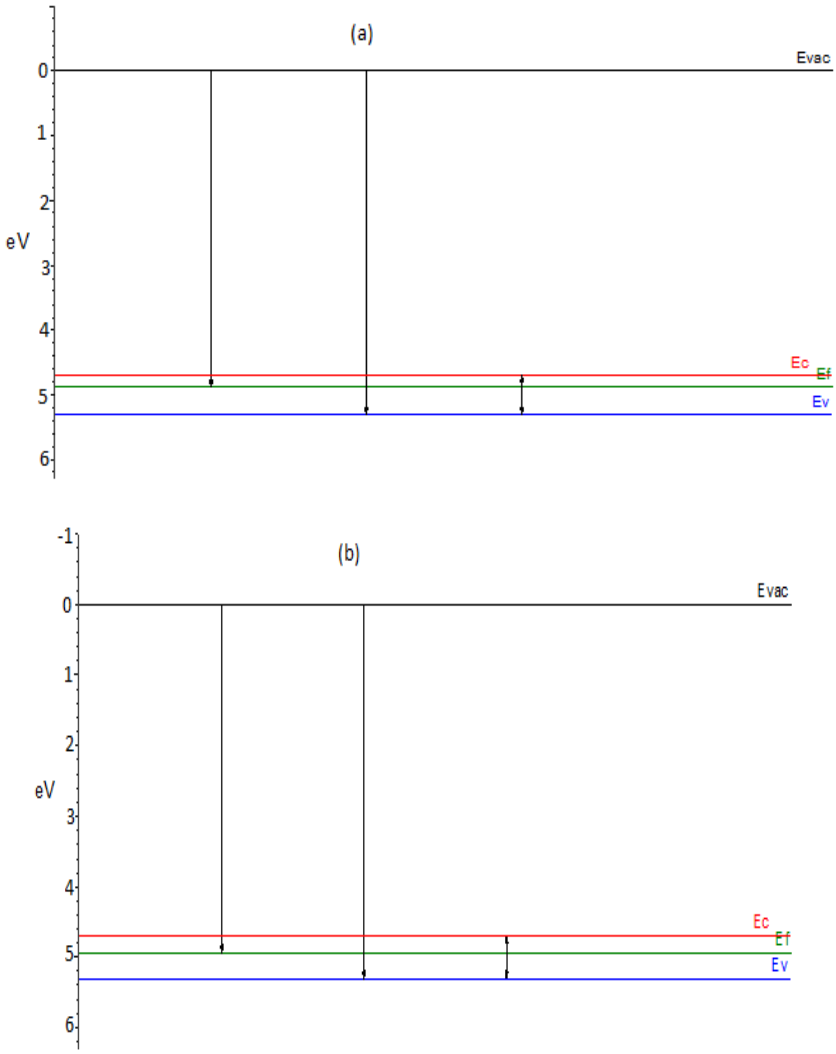

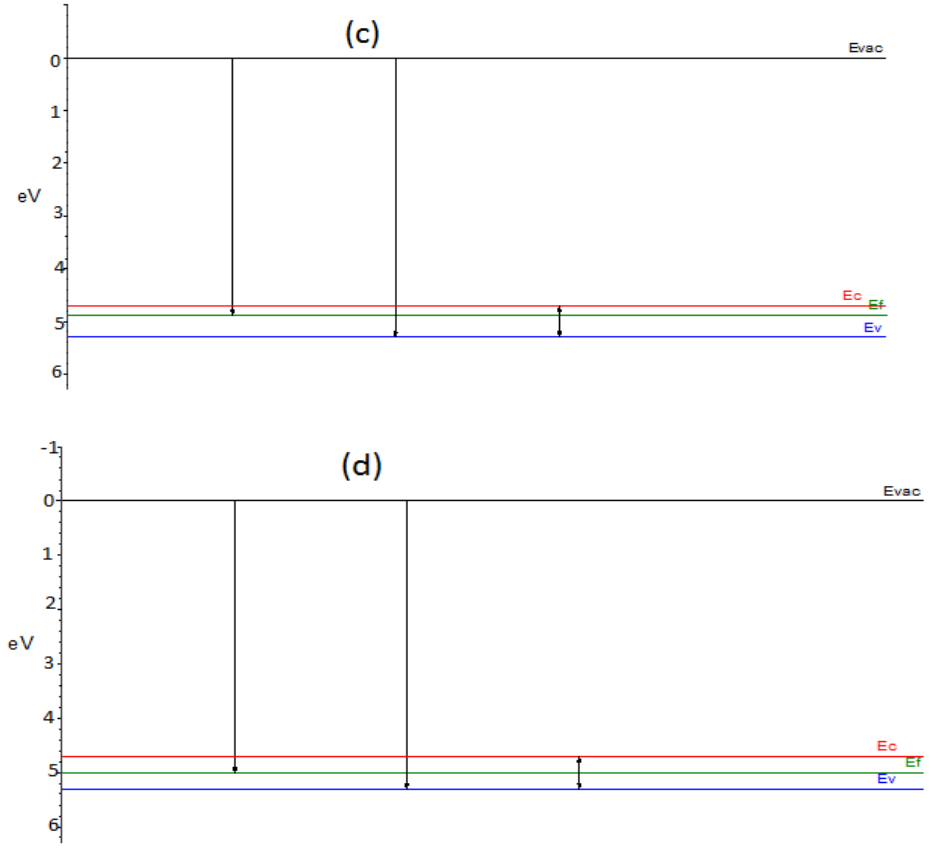

Figure 10. c) Energy band diagram for sample $Cu_{0.3}Mg_{0.70}NiFe_2O_4$. The fermi level has shifted towards the valence band, a characteristic of p-type semiconductor. d) Energy band diagram for sample $Cu_{0.45}Mg_{0.55}NiFe_2O_4$. The fermi level has shifted towards the conduction, a characteristic of an n-type semiconductor

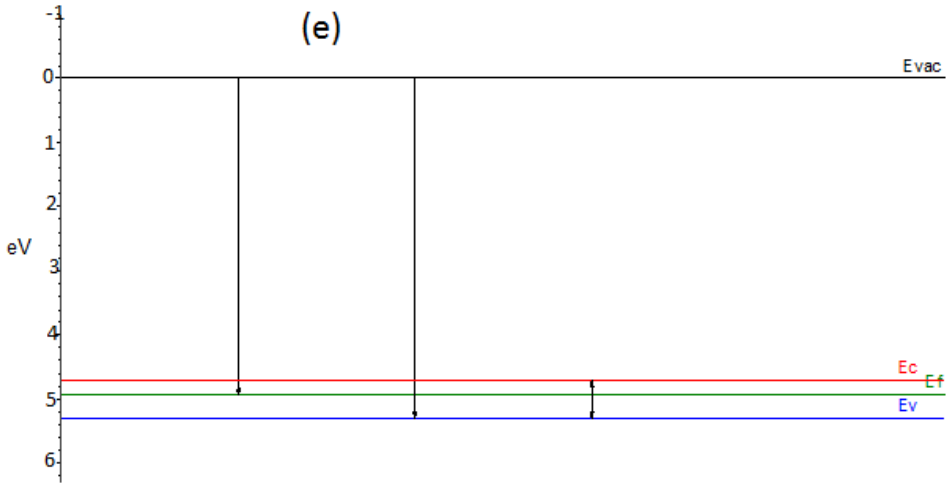

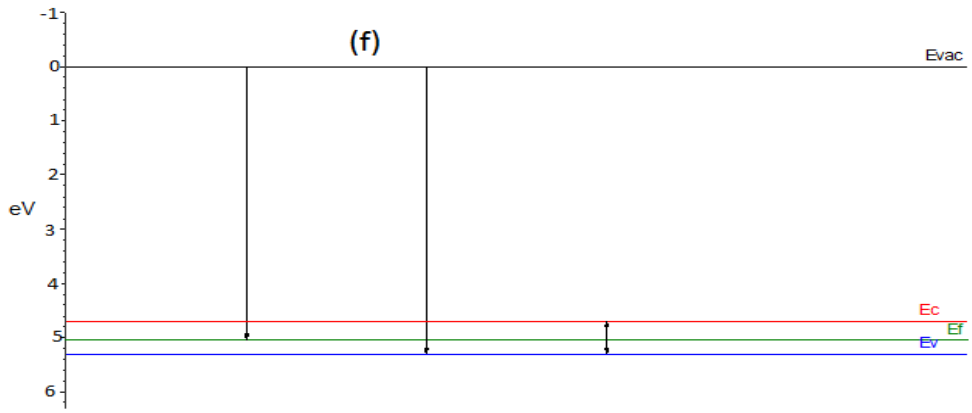

Figure 11. e) Energy band diagram for sample $Cu_{0.60}Mg_{0.40}NiFe_2O_4$. The fermi level has shifted towards the valence band, a characteristic of p-type semiconductor. f) Energy band diagram for sample $Cu_{0.75}Mg_{0.25}NiFe_2O_4$. The fermi level has shifted towards the valence band, a characteristic of a p-type semiconductor

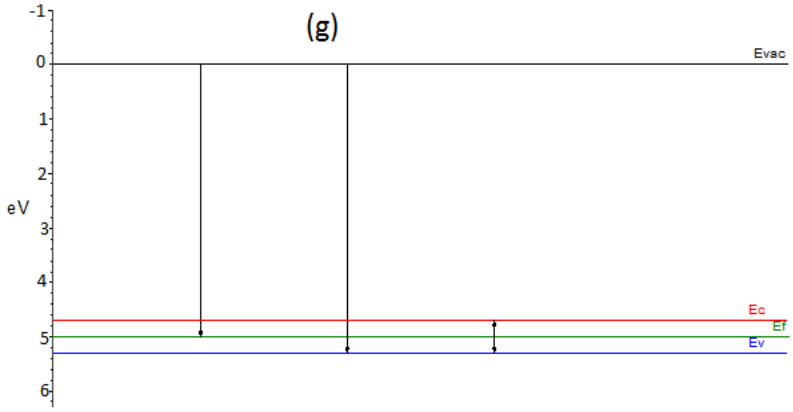

Figure 12. Energy band diagram for sample $CuNiFe_2O_4$. The fermi level has shifted towards the valence band, a characteristic of an n-type semiconductor

Figure 9–12 show a shift of the fermi level, either towards the conduction band or the valence band. The fermi level describes a level comparative to which electron concentration is specified. In case the fermi level E_f is equidistant the valence band and conduction band then, the electron density is equal to the hole density at the top of the valence band. If the fermi level is predisposed towards the conduction band, the electron bulk at the bottom of the conduction band is higher compared to that at the topmost of the valence band. It is important to note that the fermi level lies at the Dirac point. Doping introduces new energy levels within the bandgap depending on the dopant concentration or free electron concentration due to electron recombination [20]. This makes a shift fermi either towards the conduction band or the valence band [35]. The fermi level of a Dirac material is given by:

$$\chi_s = E_{C-}E_f \quad (2)$$

Where χ_s is the electron attraction, E_C the conduction band and E_f the fermi energy of the

material. The surface potential is simply the energy barrier to free space that inhibits the electron at the fermi level from leaving the surface of the material. It is bicomponent that is the bulk and the surface component which originates from a redistribution of charges at the surface of a material [20]. Surfaces or atomic arrangements could contribute to a shift in surface potential as depicted in Figures 9–12.

UV-Visible analysis

The merged spectra for the seven samples for absorbance against wavelength and energy respectively (Figure 13).

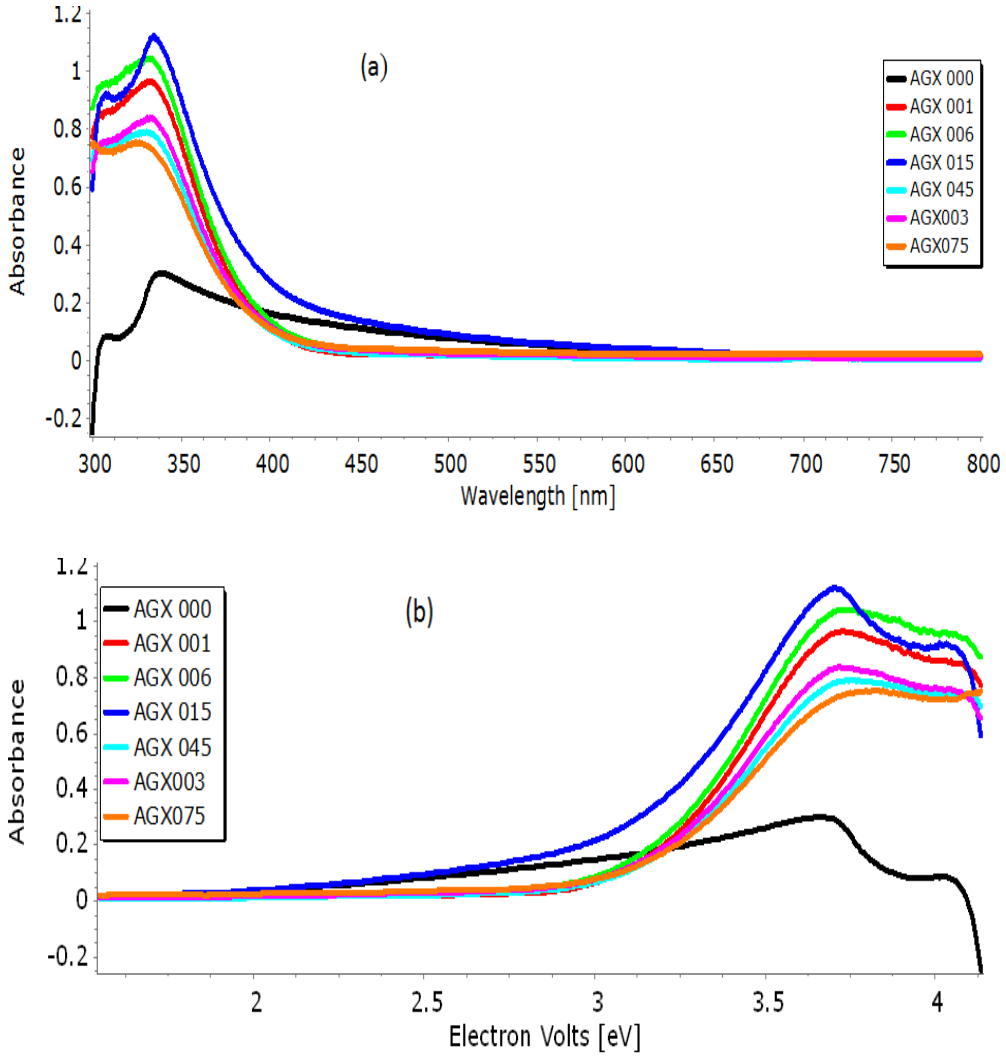

Figure 13. a) UV-Visible absorbance against wavelength spectrum. It shows a shift in wavelength and absorbance as doping was being done in $Cu_xMg_{1-x}NiFe_2O_4$ (for x=0.00, 0.15, 0.30, 0.45, 0.60, 0.75 and 1.00). The absorbance increases with a reduction in the wave. b) Absorbance versus energy band gap in electron volts for the synthesized samples. The undoped sample ($MgNiFe_2O_4$) indicates low absorbance as compared to $Cu_xMg_{1-x}NiFe_2O_4$ for (x>0) ferrite nanoparticles

All the synthesized samples portray optical properties within the ultraviolet region. For undoped $MgFe_2O_4$, the absorbance of 0.302 was recorded at a wavelength of 339 nm. UV- Visible

absorption peak shows that electrons are absorbing energy at some specific wavelength as doping proceeds. Electrons are absorbing energy implies that they are jumping to the excited state from the ground state. The material is having bandgap, thus which can be determined by absorption wavelength [36]. Doping brings about a shift in the energy band gap. Increase in absorbance causes a corresponding increase in the energy band gap. This effect could be brought by the decrease in crystalline size initiated by quantum confinement effects arising from the nano-regime. It may be also due to the additional sub-band-gap energy levels that are created by the interface and surface defects in the agglomerated nanoparticles [37].

The relationship between band gap and sample concentration for copper doped magnesium nickel ferrite nanoparticles is as illustrated in Figure 14.

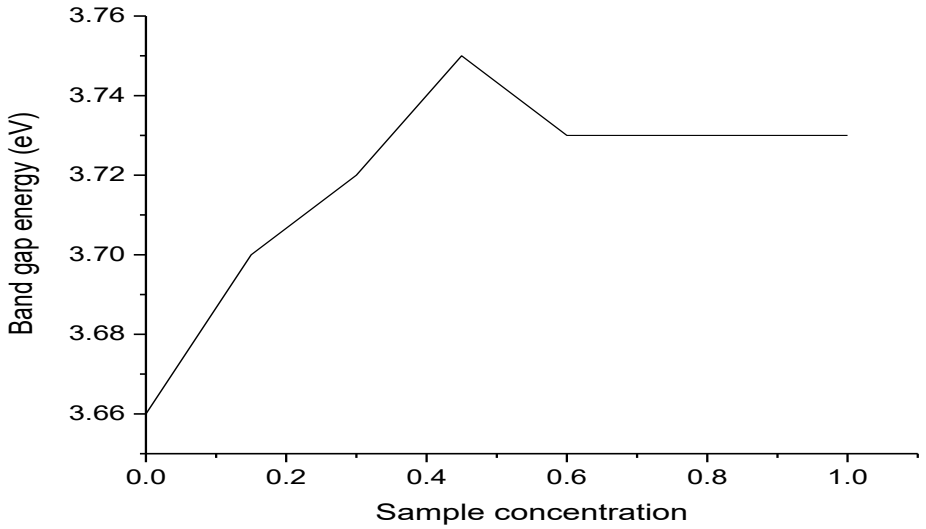

Figure 14. Concentration of the sample versus band gap energy curve for. $Cu_xMg_{1-x}NiFe_2O_4$. The band gap increases from 3.60 -3.75 eV, then decreases with a constant value of 3.73 eV

During copper doping there was observed a decrease in the wavelength. This decrease in wavelength suggests an increase in band gap [36]. The optical excitation of an electron from the valence band to the conduction band is evident by increase in band gap energy [38]. Reduction in the band gap shows that the particle size is reducing which further implies a smaller atom that constitutes the ferrite nanoparticle. The band gap was obtained using the Equation 3.

$$E = \frac{hc}{\lambda} \quad (3)$$

Where E, is the band gap energy in electron volts, h is the Planck's constant, c is the velocity of light given as and is the absorption peak wavelength. The obtained band gaps for the samples were in the range of 3.66-3.75eV. The absorbance of the synthesized samples was related to its energy band gap.

Conclusions

In this work, the optical and electronic properties of the prepared copper doped magnesium ferrite were studied. The synthesis was successfully through citra-gel auto-

combustion method to obtain copper doped magnesium nickel ferrite nanoparticle. The surface potential from Kelvins probe has been determined, for the area scan, it is in the range of 4.361-5.002 eV while for the line scan was in the range of 4.251-5.006 eV, samples with x=0.75 indicated positive work function as the others showed a negative work function. The band gap energy from the UV-Visible was in the range of 3.66-3.76 eV. The band gap is proportional to copper concentration up to sample x=0.45, which then decreases for x=0.60 and finally remains constant. Copper doping brings about variation in both the band gap and the surface potential hence a variation in optical and electronic properties. Such properties could find applications in recording, storage memory devices, and optical devises.

Disclosure Statement

No potential conflict of interest was reported by the authors

References

[1]. Khairy M., Gouda M.E. *Journal of Advanced Research*., 2015, **6**:555

[2]. Waqas H., Qureshi A.H., Subhan K., Shahzad M. *Ceramics International*., 2012, **38**:1235

[3]. Pullar R.C. *Hexagonal ferrites: Progress in Materials Science*., 2012, **57**:1191

[4]. Ikenaga N.O., Ohgaito Y., Matsushima H., Suzuki T. *Fuel*., 2004, **83**:661

[5]. Pradeep N., Sivasenthil E., Janarthanan B., Sharmila S. *In Journal of Physics: Conference Series*, 2019, **1362**:012026

[6]. Dhineshbabu N.R., Vettumperumal R., Narendrakumar A., Manimala M., Kanna R.R. *Engineering and Medicine*., 2017, **9**:377

[7]. Sardjono P., Setiabudidaya D. In *Journal of Physics: Conference Series* 2019., **1282**: 012060

[8]. Leung T.C., Kao C.L., Su W.S., Feng Y.J., Chan C.T. *Physical Review B*., 2003, **68**:195408

[9]. Iqbal S., Kotnala G., Shah J., Ahmad S. *Materials Research Express*., 2019, **6**:055018

[10]. El Maalam K., Fkhar L., Hamedoun M., Mahmoud A., Boschini F., Hlil E.K., Benyoussef A., Mounkachi O. *Journal of Superconductivity and Novel Magnetism*, 2017, **30**:1943

[11]. Bhujun B., Tan M.T., Shanmugam A.S. *Ceramics International.*, 2016, **4**:6457

[12]. Šepelák V., Baabe D., Mienert D., Schultze D., Krumeich F., Litterst F.J., Becker K.D. *Journal of Magnetism and Magnetic Materials*., 2003, **257**:377

[13]. Yadav R.S., Havlica J., Hnatko M., Šajgalík P., Alexander C., Palou M., Bartoníčková E., Boháč M., Frajkorová F., Masilko J., Zmrzlý M. *Journal of Magnetism and Magnetic Materials*, 2015, **378**:190

[14]. Cao J., Wang Y., Zhou Y., Ouyang J.H., Jia D., Guo L. *Journal of Electroanalytical Chemistry*, 2013, **689**:201

[15]. Rashad M.M., Mohamed R.M., Ibrahim M.A., Ismail L.F., Abdel-Aal E.A. *Advanced Powder Technology*, 2012, **23**:315

[16]. Hussein S.I., Elkady A.S., Rashad M.M., Mostafa A.G., Megahid R.M. *Journal of Magnetism and Magnetic Materials*., 2015, **379**:9

[17]. Joshi G.P., Saxena N.S., Mangal R., Mishra A., Sharma T.P. *Bulletin of Materials Science.*, 2003, **26**:387

[18]. Singh H., Singh J., Dosanjh H.S. *Journal of Chemical and Pharmaceutical Research.*, 2015, **7**:612

[19]. Kefeni K.K., Msagati T.A., Mamba B.B. *Materials Science and Engineering: B*, 2017, **215**:37

[20]. Kahn A. *Materials Horizons*, 2016, **3**:7

[21]. Lu H., Liu Z., Yan X., Li D., Parent L., Tian H. *Scientific Reports*., 2016, **6**:1

[22]. Tran R., Li X.G., Montoya J.H., Winston D., Persson K.A., Ong, S.P. *Surface Science.*, 2019, **687**:48

[23]. Yu B., Li M., Liu J., Guo D., Pei L., Zhao X. *Journal of Physics D: Applied Physics*., 2008, **41**:065003
[24]. Guo L., Hua G., Yang B., Lu H., Qiao L., Yan X., Li D. *Scientific Reports*., 2016, **6**:20660
[25]. Wicinski M., Burgstaller W., Hassel A.W. *Corrosion Science*, 2016, **104**:8
[26]. Melitz W., Shen J., Kummel A.C., Lee S. *Surface Science Reports*., 2011, **66**:1
[27]. Hiehata K., Sasahara A., Onishi H. *Nanotechnology*, 2007, **18**:084007
[28]. Chavan P., Naik L.R. *Physica Status Solidi (a)*, 2017, **214**:1700077
[29]. Hoffmann M.R., Martin S.T., Choi W., Bahnemann D.W. *Chemical Reviews.*, 1995, **95**:69
[30]. Dawoud H.A. *Materials Sciences and Applications*., 2011, **2**:1572
[31]. Tatarchuk T.R., Paliychuk N.D., Bououdina M., Al-Najar B., Pacia M., Macyk W., Shyichuk, A. *Journal of Alloys and Compounds*, 2018, **731**:1256.
[32]. Sadewasser S., Leendertz C., Streicher F., Lux-Steiner M.C. *Nanotechnology*, 2009, **20**:505503
[33]. Su Y., Zhang Z., Liu H., Wang Y. *Applied Catalysis B: Environmental*., 2017, **200**:448
[34]. Wan Y., Li Y., Wang Q., Zhang K., Wu Y. *International Journal of Electrochemical Science*., 2012, **7**:5204
[35]. Mishra A., Singh V.K., Mohanty T. *Journal of Materials Science*., 2017, **52**:7677
[36]. Loganathan A., Kumar K. *Applied Nanoscience*, 2016, **6**:629
[37]. Manikandan A., Vijaya J.J., Sundararajan M., Meganathan C., Kennedy L.J., Bououdina M. *Superlattices and Microstructures*, 2013, **64**:118
[38]. López R., Gómez R. *Journal of Sol-gel Science and Technology*, 2012, **61**:1

How to cite this manuscript: Gideon Osamong, Paul Kuria Kamweru*, Joel Mwangi Gichumbi, Francis Gichuki Ndiritu. Surface potential, fermi level and band gap energy of copper doped magnesium nickel ferrite nanoparticles**.** *Asian Journal of Nanoscience and Materials*, 4(1) 2021, 1-14. DOI: 10.26655/AJNANOMAT.2021.1.1